CURRENT SHEET THICKNESS IN THE NEAR-EARTH PLASMA SHEET DURING SUBSTORM GROWTH PHASE AS INFERRED FROM SIMULTANEOUS MAGNETOTAIL AND GROUND-BASED OBSERVATIONS

V. A. Sergeev,* P. Tanskanen,** K. Mursula,** A. Korth*** and R. C. Elphic †

* *Institute of Physics, Leningrad State University, Leningrad 198904, U.S.S.R.*
** *Department of Physics, University of Oulu, Finland*
*** *Max-Planck-Institut für Aeronomie, Katlenburg-Lindau, F.R.G.*
† *Institute of Geophysics and Planetary Physics, University of California, Los Angeles, CA 90024, U.S.A.*

ABSTRACT

Multi-point magnetic field measurements made by spacecraft in the tail region during the growth phases of two substorms were used to model the magnetic configuration in the location conjugate to the Scandinavian riometer and magnetometer network. Assuming the origin of the observed southward moving band of energetic electron precipitation as due to pitch-angle scattering in the equatorial current sheet, we inferred the half-thickness of the current sheet at $r \approx 9\ R_E$ as thin as 0.1 R_E near the end of the growth phase. Combined with the modelled evolution of the magnetic configuration, this mechanism consistently explains the main features of the electron precipitation.

INTRODUCTION

The increase of the tail current, the stretching of the field lines and the plasma sheet thinning are the most spectacular signatures of the substorm growth phase seen in the magnetotail /1-3/. The half-thickness (D) of the current sheet is one of the parameters controlling the substorm expansion phase onset /4-5/. The direct estimate of this parameter requires multi-spacecraft observations. In a recent study /6/ this parameter was found to decrease from about 5 R_E to less than 1 R_E at $r \approx 13\ R_E$ during the first 20 minutes of a very strong growth phase.

In this paper we report on simultaneous magnetotail and ground-based measurements. The magnetic measurements in the tail are used to map the field lines from the magnetosphere to the ionosphere. On the other hand, the ground-based registration of precipitated energetic electrons, used as tracers of conditions on the equatorial field lines, allows to estimate the current sheet thickness in some flux tubes. In verification, we shall also compare basic properties of the energetic particle precipitation inferred from our model calculations with those known from observations.

OBSERVATIONS

Two similar premidnight substorm growth phases are studied. Two spacecraft were in both cases located in the 22-23 MLT sector, suitable for comparison with observations from the ground network. GEOS-2, used in both events, was in a geosynchronous orbit, with its nominal conjugate point in northern Scandinavia. The event on 23 May 1979 (Figure 1) was initiated by an increase in the IMF southward component after 18 UT (data not shown). The tailward stretching of the magnetic field lines during the growth phase was seen on ISEE-1 and Geos-2. The expansion phase onset at 20:18 UT was evidenced by poleward expanding CNA and by the increase of B_z at ISEE-1.

The event on 23 June 1979 (Figure 2) had an expansion phase onset at 21:01 UT /7/. The IMP-J spacecraft was located in the southern tail lobe at $r \approx 33\ R_E$ and recorded an increase in the lobe field from 20 nT at 20 UT up to 25 nT at 21 UT. During the growth phases of both events, a southward moving CNA region was detected by the riometers at Kevo and Ivalo stations (Table 1). From a 18-20 min delay in peak absorption over Kevo and Ivalo, a southward drift speed of about 0.06-0.07°/min was estimated. When the CNA peak was over Kevo/Ivalo, the H-component at GEOS-2 had the values of 74/67 nT and 76/65 nT, respectively.

SIGNATURES OF THE ENERGETIC ELECTRON PRECIPITATION

Meridional distributions of trapped and precipitating particles (Figure 3) are used to probe the magnetic field configuration in the nightside magnetosphere /8-10/. It can be seen that: a) the largest precipitation of radiation belt particles that is isotropic over the loss cone is seen in the outer portion of the radiation belt outside some boundary (here called the isotropic boundary, IB); b) IB is rather sharp and thin; c) position of IB depends on particle rigidity G (G = mV/e ; V is the total velocity of the particle) and is displaced more earthwards in the magnetotail for particles of higher rigidity. The IB position for energetic electrons corresponds to the region of their maximum precipitation and may be determined using e.g. CNA and X-ray observations. The maximum effect on CNA is expected from 30 to 150 keV electrons /11/. The corresponding threshold rigidities are 600 and 1400 nT km, respectively.

According to recent models developed for particles mirroring near the ionosphere /12-14/, the IB position is expected to be on those flux tubes which meet the following condition in the central plane of the equatorial current sheet:

$$K_C \equiv R_C/\rho = B_z^2 \Big/ G\frac{\partial B_x}{\partial z} \qquad (1)$$

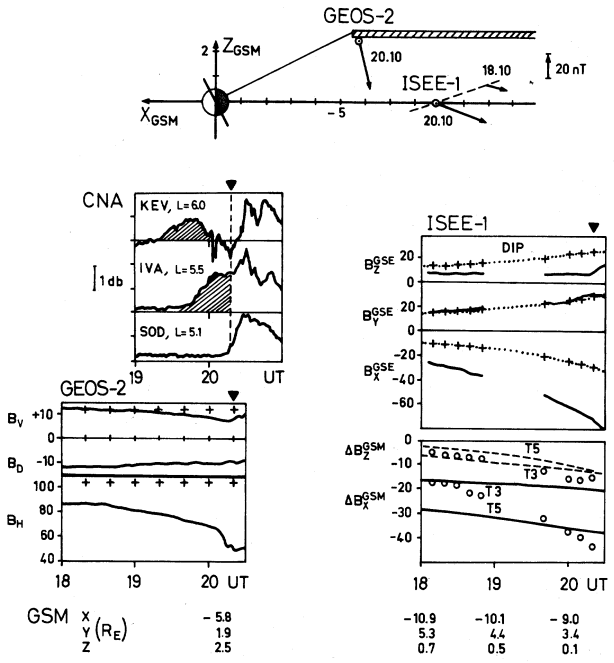

Fig.1. Observations on 23 May 1979. Black triangles indicate expansion onset at 20:18 UT. Top: Spacecraft configuration and the measured external magnetic field vectors in the x-z plane. The narrow hatched area indicates the approximate current sheet location. Mid-left: CNA amplitudes at the Finnish riometer chain. Left down: Magnetic field (in nT) measured by GEOS-2. Dipole field is shown by crosses. Mid-right: Magnetic field measured by ISEE-1. Right down: The x- and z-components of the external magnetic field measured by ISEE-1 (circles) and calculated in two variants (K_p = 3, line T3 and K_p = 5, line T5) of the Tsyganenko model.

A local orthogonal coordinate system is used where z is perpendicular to the current sheet and x is directed along the magnetic field outside the current sheet. R_c is the field line curvature radius at the equator and $\rho = G/B_z$. K_c is about 8 for the given range of rigidities (of the order of 1000 nT km). From equation (1) it is found that the decrease of the current layer thickness and B_z in the tail will move the IB position inside the radiation belt. As the field lines are stretched, the latitude of the ionospheric projection of a fixed point in the magnetosphere decreases, giving rise to the southward drift of the precipitation region. We interprete the maximum CNA (or X-ray) amplitude as a signature of IB position.

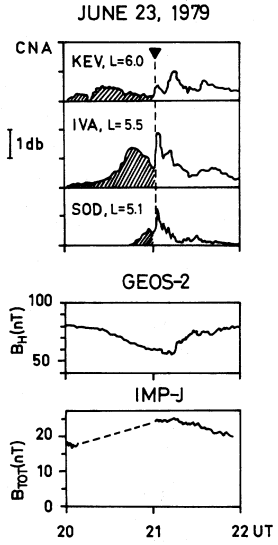

Fig.2. Observations on 23 June 1979. Top: CNA amplitudes. Center: H-component as measured by GEOS-2. Bottom: Total magnetic field in the southern lobe measured by IMP-J at GSM x,y,z = [-26,-9,-17] R_E.

Station or balloon	Abbr.	Corrected Lat	geomagnetic Long	May 23, 1979 onset(UT)	max	max CNA (db)	June 23, 1979 onset(UT)	max	max CNA (db)
KA0622	K22	69.7	87.7				19:45	19:50	weak X ray peak
Dixon	DIX	67.75	155.7	no CNA observed			no CNA observed		
Andoya	AND	66.31	102.6					20:23	1.7
Kevo	KEV	66.00	111.2	19:20	19:45	0.9	20:00	20:27	1.0
Leirvogour	LEI	66.00	69.5	19:42	20:12	0.8	20:22	20:40	
S00622	S22	65.64	93.1				20:10	20:36	intense X ray peak
Ivalo	IVA	64.83	110.5	19:45	20:03	1.7	20:25	20:47	1.4
Ugorskiy Shar	USH	64.48	137.7	19:40	20:00	1.7	20:20	20:(40...50)	1.2
Sodankylä	SOD	63.73	108.9	not observed until exp. onset			20:45	growing up to exp.onset	
S00623	S23	63.44	109.5				20.55	-"-	

Table 1. CG coordinates of ionospheric points above riometers and balloons. Onset and maximum precipitation times and the maximum CNA magnitudes are also shown.

MODELLING THE MAGNETIC FIELD CONFIGURATION

We use the field model by Tsyganenko /15/, hereafter called T87, to interpolate the external B_z field beyond the points measured by GEOS-2 and ISEE-1. The sources of the external (dipole field subtracted) field $\Delta\vec{B}$ are as follows:

$$\Delta\vec{B}(r) = \vec{B}_{DCF} + \vec{B}_{DR}(DR, \rho_0) + f\vec{B}_T(J^{K_p}(x), XN, D, DM) \qquad (2)$$

The effects of the currents at the dayside magnetopause (DCF) plus all other effects not included in the ring current (DR) and the tail current (T), were represented by polynomial expansions and have been determined from the extensive experimental data set in T87. They are retained in B_{DCF}. The DR contribution depends on the radius of DR current (ρ_0) and the ring current field intensity (DR), adjusted to the conditions of that day. Using the Dst value of -18 nT and a correction for the solar wind dynamic pressure in the form DR(nT) = Dst(nT) - 0.024 $\sqrt{n}V^2$, where n (cm^{-3}) and V (km/s) are the solar wind density and velocity, we estimate DR ≈ -40 nT.

The tail currents in T87 are the plasma sheet current plus its closure currents at the magnetopause. The sheet current is composed of finite size current filaments having an intensity decreasing with distance from the Earth. These radial profiles of linear current density $J^{K_p}(x)$ have been determined in T87 for a few groups of activity levels (parametrized by K_p index). The factor f allows the total tail current to be changed.

As the first modification to the T87 model we introduce the inhomogeneous thinning of the current sheet (Figure 4) in the form: D(x) = 0.5 * (D + DM + (D - DM) * cos (2π * (x /18 + 1)) . The position of the first minimum half-thickness DM was fixed at x = -9 R_E. The half-thickness smoothly increases to its maximum value D at x = -18 R_E.

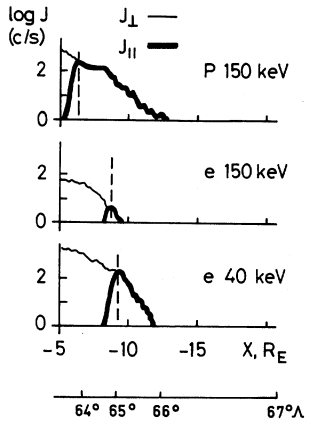

Fig.3. Fluxes of precipitated ($J_{||}$) and trapped ($J_{\perp}$) energetic protons (p) and electrons (e) at the nightside against the invariant latitude Λ and the equatorial x-values corresponding to the time at 20:10 UT on 23 May1979.

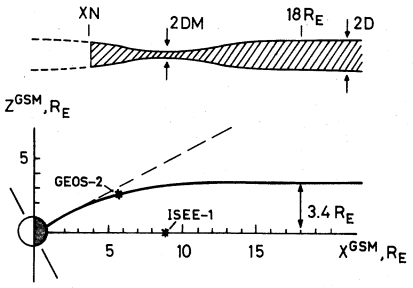

Fig.4. Configuration of the current sheet thickness and the geometry of the curved current sheet plane used in model calculations.

The inner edge of the current sheet (XN) is one more parameter to be determined. The second modification concerns the geometry of the "neutral sheet" (center plane of the current sheet near midnight). Assuming that the neutral sheet joins the magnetic equator at $r \leq 4\ R_E$ /16/ and that its height from the equatorial plane at $x \leq -10\ R_E$ is about $7.5\ R_E * \sin \Psi$ /14/, where Ψ is the angle of dipole tilt to the Sun, then, for the particular time at 20:10 UT on 23 May 1979, the neutral sheet surface at $x \geq -11.74\ R_E$ is approximated as a parabola: $z = 3.4 - 0.0247\ (x+11.74)^2$. In this geometry GEOS-2 is located close to the neutral sheet surface, in agreement with magnetic observations. This model was used to calculate the magnetic field during the 23 May 1979 event using the free parameters f, XN, D and DM. A set of field models was identified giving a fit within 1-2 nT to the observed values of B_z at both spacecraft and of B_x at ISEE-1 (Table 2). A reasonable agreement between the model and observations was found for $K_p = 3$.

ESTIMATE OF THE CURRENT SHEET THICKNESS

For all selected models we calculated the configuration of magnetic field lines anchored in the ionosphere along 110° CGLong magnetic meridian. The results indicate that the latitudes of the ionospheric projections of fixed magnetospheric points agree to within 0.2° CGLat. Figure 5 shows that the projection of the ionospheric point above Ivalo to the current sheet falls at $r = (9.0 \pm 0.5)\ R_E$ in all cases. The corresponding latitude versus rigidity profiles, as calculated from Eq. (1), are very dependent on the current sheet thickness. If the IB position of 30 keV electrons is to be projected to (or southward of) Ivalo, the current sheet thickness is not less than $0.1\ R_E$. At the time of the CNA maximum at Kevo (19:45 UT), the best fit was found for $DM = 0.1\ R_E$. The corresponding equatorial IB position, projected from the ionospheric point over Kevo was at $r = 9.8\ R_E$ (Table 2 and Figure 5).

The average equatorial IB position for 40 keV electrons during growth phase is at $r = 18\ R_E$ and about 69° CGLat in the midnight sector (T87). This position is just outside the outer boundary of pseudo-trapping region, the drift shell of particles mirroring near the ionosphere. According to /17/, this region cannot contain measurable fluxes of energetic electrons in quiet conditions. By the same reason, we do not expect to see any measurable CNA at stations like Dixon, slightly to the south of the estimated ionospheric projection of the IB at the beginning of the growth phase (Table 1).

DISCUSSION

Buck et al. /18/ have reported on observations of a fast thinning wave which flattens the gyrocenters of energetic ions into the layer of about $0.1\ R_E$ thickness. These observations were made at the end of a growth phase event at $r \approx 8\ R_E$ and about $1\ R_E$ above the neutral sheet. The isotropization of the energetic electron distribution without accompanying increase in wave activity was reported by West et al. /19/. These observations agree with ours. West et al. /14/found an excellent agreement between the calculated and observed position of the isotropic boundary. They also found the $1\ R_E$ half-thickness for the current sheet and the $11\ R_E$ distance for IB of 80 keV electrons at the equator.

The CNA intensity in the center of the southward moving CNA band displays an evident increase during the growth phase. The inward IB motion towards flux tubes containing higher particle fluxes offers a natural explanation to this feature. Our model shows that the temporal evolution of the magnetic field during the growth phase is the main cause for the observed southward motion of the precipitation region. About 80 % of the meridional displacement from Kevo to Ivalo between 19:45 and 20:03 UT on 23 May 1979 is due to the tailward stretching of the field lines while the remaining 20 % is due to the earthward motion of the source region at the equator (Figure 5).

A hard auroral X-ray spectrum at the beginning of an event as recorded by balloons, followed by the steadily softening spectrum during the maximum stage and at the end of the precipitation event /7/, can be explained by the rigidity dependence of the IB position. According to Figure 5, the region between isotropic boundaries of 30 keV and 150 keV electrons, i.e. the region of hard precipitation, is expected to have a 0.3-0.4° CGLat width along the meridian.

May 23, 1979	GEOS-2			ISEE-1			model					
UT	B_x	B_y	B_z	B_x	B_y	B_z	K_p	f	XN	DR	D	DM
20:10	-12.	+8.	-41.6	-39.0	7.2	-16.0		measured				
	-8.7	-1.4	-42.2	-39.5	0.1	-17.0	3	1.7	-2.8	-45.	1.	0.1
	-8.6	-1.4	-41.7	-39.4	0.1	-17.0	3	1.7	-2.8	-45.	1.	0.2
	-8.4	-1.4	-40.8	-39.2	0.1	-17.0	3	1.7	-2.8	-45.	1.	0.4
	-8.8	-1.4	-39.5	-39.4	0.1	-17.7	3	1.75	-2.8	-45.	1.	1.
19:45	-8.	+7.	-33.6	-32.5	4.6	-13.2		measured				
	0.4	-2.1	-35.4	-32.9	-0.5	-11.5	3	1.5	-2.4	-35.	1.	0.1
18.30	-2.	+9.	-23	-18.3	3.0	-6.8		measured				
	1.6	-4.2	-24.3	-17.1	-0.4	-7.2	3	1.0	-3.7	-40.	2.07	2.0

Table 2. GSM coordinates of external magnetic field measured by GEOS-2 and ISEE-1, and calculated for a few best fit models.

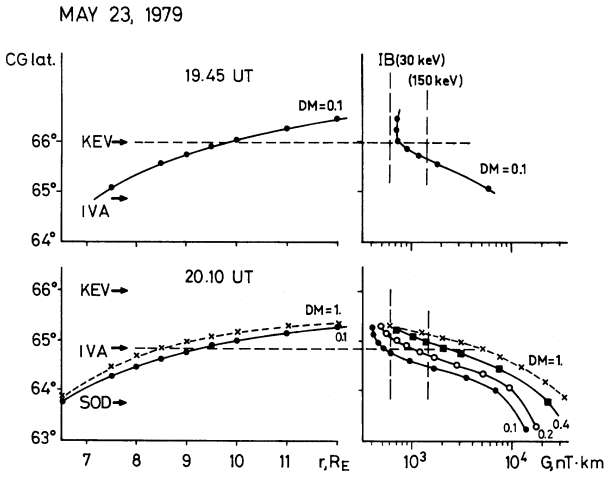

Fig.5. Correspondence between ionospheric and equatorial positions of flux tubes at 110° CGLong meridian (left) and between latitude and critical IB rigidities (right) for a few of the models given in Table 2.

The progressive hardening of the energy spectra in the course of the growth phase /7/ reflects the softening of the energy spectrum of energetic electrons when moving towards the outer edge of the radiation belt /20/. The reason for such a spectral variation of the radiation belt electrons is the faster drift-cone loss of the more energetic particles in the pseudo-trapping region /17/.

CONCLUSIONS

Our results illustrate in a quantitative manner the time evolution of the magnetic configuration in the night sector of the near-Earth tail during the substorm growth phase. This evolution seems to be the main factor leading to the well-known equatorward expansion of the auroral oval.

Interpreting the observed precipitation of energetic electrons in terms of particle pitch-angle diffusion in the equatorial current sheet we were able to estimate the current sheet half-thickness at the end of the growth phase to be about 0.1 R_E at $r \approx 9\ R_E$. It is suggested that the flattened current sheet at $r \approx 10\ R_E$ is embedded within a broad (few R_E) plasma sheet. Referring to the recent theoretical results by Büchner and Zeleny /5/ we conclude that the magnetic configuration at the end of the growth phase is very close to being unstable against the explosive tearing mode instability.

REFERENCES

1. Russell, C. T., and R. L. McPherron, Space Sci. Rev. 15, 205 (1973)
2. Nishida, A., and K. Fujii, Planet. Space Sci. 24, 849 (1976)
3. Fairfield, D. H., R. P. Lepping, E. W. Hones, S. J. Bame, and J. R. Asbridge, J. Geophys. Res. 86, 1396 (1981)
4. Schindler, K., and J. Birn, J. Geophys. Res. 87, 2263 (1982)
5. Büchner, J., and L. M. Zeleny, Sov. J. Plasma Physics 13, 109 (1987)
6. McPherron, R. L., A. Nishida, and C. T. Russell, in: Quantitative modelling of magnetosphere-ionosphere coupling processes, ed. Y. Kamide, Kyoto, Japan 1987, p. 252
7. Tanskanen, P., J. Kangas, L. Block, G. Kremser, A. Korth, J. Woch, I. B. Iversen, K. M. Torkar, W. Riedler, S. Ullaland, J. Stadnes, and K.-H. Glassmeier, J. Geophys. Res. 92, 7443 (1987)
8. Fritz, T. A., J. Geophys. Res. 75, 5387 (1970)
9. Imhof, W. L., J. B. Reagan, and E. E. Gaines, J. Geophys. Res. 84, 6371 (1979)
10. Lundblad, J. A., F. Søraas, and K. Aarsnes, Planet. Space Sci. 27, 841 (1979)
11. Collis, P. N., and A. Korth, J. Atmos. Terr. Phys. 47, 327 (1985)
12. Sergeev, V. A., E. M. Sazhina, N. A. Tsyganenko, J. A. Lundblad, and F. Søraas, Planet. Space Sci. 31, 1147 (1983)
13. Sergeev, V. A., and M. V. Malkov, Geomagnetizm i Aeronomiya 4, 649 (1988)
14. West, H. I., R. M. Buck, and M. G. Kivelson. J. Geophys. Res. 83, 3819 (1978)
15. Tsyganenko, N. A., private communication (1987)
16. Fairfield, D. H., M. H. Acuna, L. J. Zanetti, and T. A. Potemra, J. Geophys. Res. 92, 7432 (1987)
17. Sergeev, V. A., and N. A. Tsyganenko, Planet. Space Sci. 30, 999 (1982)
18. Buck, R. M., H. I. West, and R. G. D. D'Arcy, J. Geophys. Res. 78, 3103 (1973)
19. West, H. I., R. M. Buck, and J. R. Walton, J. Geophys. Res. 78, 3093 (1973)
20. McDiarmid, J. B., and A. Hruska, J. Geophys. Res. 77, 3377 (1972)